ChemistrySelect

Research Article
doi.org/10.1002/slct.202404665

Chemistry Europe
European Chemical Societies Publishing

www.chemistryselect.org

Revisiting Metal Dihalide Complexes with Phosphine Ligands: Isostructurality, Steric Effects, Anagostic Interactions, Crystal Voids, and Energetic Calculations

Hiram Pérez,*[a] Diego M. Gil,[b] Rosa M. Gomila,[c] and Antonio Frontera*[c]

The crystal structures of seven metal dihalide complexes with triphenylphosphine (PPh_3) and two with tribenzylphosphine (PBz_3) have been reanalyzed. The studied complexes include $[FeCl_2(PPh_3)_2]$, $[CoCl_2(PPh_3)_2]$, $[CoBr_2(PPh_3)_2]$, $[NiCl_2(PPh_3)_2]$, $[NiBr_2(PPh_3)_2]$, $[NiI_2(PPh_3)_2]$, $[ZnCl_2(PPh_3)_2]$, $[NiCl_2(PBz_3)_2]$, and $[NiBr_2(PBz_3)_2]$. A detailed geometric analysis revealed high isostructurality among several pairs. Ligand steric effects were assessed using cone angles and percentage surface coverage. Crystal packing is stabilized by weak C—H⋯π and C—H⋯X (X = Cl, Br, and I) interactions. Notably, $[NiCl_2(PBz_3)_2]$ and $[NiBr_2(PBz_3)_2]$ feature rare intramolecular C—H⋯Ni anagostic interactions. Reduced density gradient (RDG) and noncovalent interaction (NCI) plots confirmed weakly attractive C—H⋯π contacts in all complexes. Void-volume analysis assessed the mechanical strength of the crystals, while pixel energy and energy frameworks clarified structural stability and dominant interactions. Density Functional Theory (DFT) calculations, along with QTAIM/NCIplot and NBO analyses, as well as electron density (ED) versus electrostatic potential (ESP) plots, were performed to better understand the C—H⋯Ni interactions and distinguish between agostic and anagostic interactions.

1. Introduction

It is well-known that the phosphine-based ligands are valuable compounds that exhibit a wide range of applications. For example, the tertiary phosphine complexes of nickel, palladium, and platinum have interest in organometallic chemistry, particularly in catalysis as homogeneous catalysts and coupling reactions.[1] On the other hand, those complexes are found to show prominent bioactivity antiviral, antifungal, antibacterial, and antitumor.[2] However, their use as anticancer drugs is limited due to the easily dissociation of these complexes in solution forming very reactive species. Diverse authors have suggested that this problem could be overcome if the complexes are stabilized by bulky ligands such as triphenylphosphine.[3]

In the triphenylphosphine-containing complexes, the conformation of the phenyl rings often contributes to the bulkiness of the complex, which is interesting because the bulkiest part of the molecule generally determines its shape and reactivity.[4] The influences of steric effect of a ligand on the structures and reaction rates of organometallic and coordination compounds have been widely discussed in the literature.[5,6] The "exact" cone angle (θ°) and the "exact" solid angle (Ω°) have been recently presented as new ligand steric descriptors[7–9] based on the idea of covering the ligand in the most acute possible cone, and evading the inaccuracy of several empirical parameters that were assumed by Tolman.[5] Other descriptors currently used for quantifying steric demand are the solid cone angle (θ°) and solid angle (Ω),[6b] the former derived from the area filled by the ligands on the surface of a sphere centered at the metal atom, and the latest associated to the shadow cone of a ligand supposedly illuminated from the metal center. The solid angle (Ω) can be calculated to quantify the total steric shielding through the so-called G-parameters.[10]

In view of all the abovementioned, and from an initial idea of extending the structural study of *trans*-dichloro-bis(tribenzylphosphine)nickel(II), $Ni(PBz_3)_2Cl_2$, previously reported for one of us,[11] we have identified a series of seven metal dihalide-complexes with triphenylphosphine ligand, and one with tribenzylphosphine ligand from CSD (version: 2023),[12] namely,
trans-dichlorobis(triphenylphosphine)iron(II), $Fe(PPh_3)_2Cl_2$,[13]
trans-dichlorobis(triphenylphosphine)cobalt(II), $Co(PPh_3)_2Cl_2$,[14]
trans-dibromobis(triphenylphosphine)cobalt(II), $Co(PPh_3)_2Br_2$,[14]
trans-dichlorobis(triphenylphosphine)nickel(II), $Ni(PPh_3)_2Cl_2$,[15]
trans-dibromobis(triphenylphosphine)nickel(II), $Ni(PPh_3)_2Br_2$,[16]
trans-diiodobis(triphenylphosphine)nickel(II), $Ni(PPh_3)_2I_2$,[17]
trans-dichlorobis(triphenylphosphine)zinc(II), $Zn(PPh_3)_2Cl_2$,[18]

---

[a] Prof. Dr. H. Pérez
Departamento de Química General e Inorgánica, Facultad de Química, Universidad de La Habana, Ciudad de la Habana 10400, Cuba
E-mail: hiramperezperez49@gmail.com

[b] Prof. Dr. D. M. Gil
Instituto de Química Orgánica. Facultad de Bioquímica, Química y Farmacia, Universidad Nacional de Tucumán Ayacucho 471, San Miguel de Tucumán T4000INI, Argentina

[c] Prof. Dr. R. M. Gomila, Prof. Dr. A. Frontera
Departamento de Química, Universitat de les Illes Balears, Crta de Valldemossa, Palma de Mallorca 07122, Spain
E-mail: toni.frontera@uib.es

Supporting information for this article is available on the WWW under https://doi.org/10.1002/10.1002/slct.202404665

trans-dichlorobis(tribenzylphosphine)nickel(II), $Ni(PBz_3)_2Cl_2$,[19] *trans*-dibromobis(tribenzylphosphine)nickel(II), $Ni(PBz_3)_2Br_2$.[19]

Hereafter these complexes are labeled by CSD refcodes, GATXOP, BIHGEE, BIHGII, CLTPNI03, BPOLEX, ZZZKQO01, GUXVAW, XEGZIS01, and GAHLOR, respectively. The main goal of the present work is revealing important structural features, which have not been studied at present in that series of nine complexes, such as: (i) isostructurality, using geometric descriptors from different sources, which allows fine-tuning of crystal properties with the final aim to prepare new materials with desired properties; (ii) the steric demand of the two bulky phosphine ligands, performing calculation of ligand cone angles from the atomic coordinates observed in the crystal structures; (iii) intramolecular anagostic interactions, which are believed to be important due to possible influences on the mechanism of C—H activation, catalytic applications, and receptor properties of these complexes;[20–22] and (iv) noncovalent interactions, which play an essential role in supramolecular chemistry, molecular biology, and crystal engineering.[23] In absence of strong hydrogen bonds, other kind of noncovalent interactions can be dominant and therefore, responsible for crystal stability.[24] A detailed study of weak intermolecular C—H···π interactions and C—H···X hydrogen bonds that control the crystal packing stability in the complexes under study is accomplished by geometric descriptors, Hirshfeld surfaces, NCI-plots, crystal void analysis, and energy frameworks.

A recent approach[25] and its extension to transition-metal coordination compounds[26] is carried out to calculate interaction energies in molecular pairs involving different structural motifs. The results are visualized using energies framework diagrams.[27] Crystal structures of the molecular species are also compared each other, thus allowing investigation on the effects of systematic metal and substituent variation. These studies are complemented by diverse computational methods in order to elucidate the nature of anagostic contacts. Based on the well-known structure-property relationship, we hope that the present work could give insights into the above cited problem on the ready dissociation attributed to these complexes, and its resulting limited effect on pharmacological targets. Also, this study could be useful for ligand design in catalytic C—H bond functionalization.

2. Methods

2.1. Description of Isostructurality

In order to estimate isostructurality various geometric descriptors were computed:

(a) Unit-cell similarity index π,[28] based on axial ratios, given values almost zero for great similarity;
(b) Isostructurality index $I_i(n)$ (in %),[28] based on distance differences between the crystal coordinates of identical non-H atoms, the larger percentages being associated to higher isostructurality. These calculations for the pairs of similar crystal structures were performed using ISOS software.[29]
(c) Degree of lattice distortion (*S*) is the spontaneous strain (sum of the squared eigenvalues of the strain tensor divided by 3);
(d) Measure of similarity (Δ) is a function of the differences in atomic positions (weighted by the multiplicities of the sites) and the ratios of the corresponding lattice parameters of the structures.[30] These two calculations were performed using COMPSTRU software.[31] The program transforms the Structure 2 to the most similar configuration of Structure 1.
(e) Packing similarity PS_{ab} using CrystalCMP.[32]This approach has been recently introduced for the comparison of molecular packing and the identification of identical crystal structure motifs. The packing similarity is calculated using a simple formula involving distance–displacement and angle–displacement of molecules inside a finite molecular cluster. Similarity matrixes and dendrograms are automatically calculated and shown. A smaller value of PS_{ab} indicates a greater degree of structural similarity. Clusters A and B are initially aligned to give the least-squares distance overlay of the atoms in the kernel molecules, then the remaining molecules in A and B are mapped by identifying the shortest distances between their centroids. A search fragment must be defined to compare molecules, and the PS_{ab} value incorporates an RMSD measure between corresponding atoms. The final PS_{ab} value is based on all (usually 15) mapped molecules.
(f) Dissimilarity index "X"[33] by using of Xpac2.0.2,[33a] a software that compares representative lists of internal coordinates-distances, intermolecular angles, dihedral angles, and torsion angles. The Xpac method allows the identification of similar packing arrangements present between two crystal structures.[33b] Common structural motifs present in crystal structures to be compared are termed as "supramolecular constructs" (SCs), which represent subcomponents of complete crystal structures. The SC may be 0D similarity, 1D similarity (row of molecules match), 2D similarity (layer of molecules match), and 3D similarity (isostructural). Xpac defines the dissimilarity index "*X*" as a measure of how far the two crystal structures deviate from perfect geometrical similarity.[33c,d] The lowest value for *X* indicates the highest degree of similarity. *X* values smaller than 1 are found for SCs with high similarity, whereas SCs of low-degree similarity produce *X* values of 6 or even higher. Stretch parameter *D* (in Å), as well as the delta(*a*)/delta(*p*) and *X*/delta(d) plots (a = angular deviation, p = interplanar angular deviation, and d = molecular centroid distance deviation) in the results window will also give an indication of the appropriate level for these parameters.

2.2. Computation of Ligand Steric Demand

Exact cone (θ°) and exact solid cone (θ°) angles were computed using the mathematica packages FindConeAngle[7] and FindSolidAngle,[9] respectively. The solid angles Ω, and G-parameters: G(L) = the percentages of metal coordination sphere shielded by each ligand, G(complex) = the G value for the complex with all ligands treated as one cumulative ligand, and G(M) = percentage of metal surface shielded only by the ligated atoms were calculated with Solid-G software[10] using zero energy point radii (r_Z) instead of the van der Waals radii.[11] All the steric parameters presented in this work were calculated based on experimental crystallographic data.

2.3. Hirshfeld Surfaces and Crystal Voids

The calculations of Hirshfeld surfaces[34] using the novel CrystalExplorer 21.5,[35] provide additional insight into weak intermolecular interactions contributing to the packing of molecules in crystals. The surfaces are mapped with the shape-index property, which is a qualitative measure of shape and is sensitive to subtle changes in surface shape, particularly in a flat region. Two shape indices differing by sign represent complementary "bumps and hollows". The donor of an intermolecular interaction is associated to blue bump-shape and shape-index >1, whereas a red hollow with index <1 represents the acceptor. A void analysis is performed by adding up the electron densities of the spherically symmetric atoms contained in the asymmetric unit.[36a] The void surface is defined as an isosurface of the procrystal electron density and is calculated using CrystalExplorer21.5 for the whole unit cell where the void surface meets the boundary of the unit cell and capping faces are generated to create an enclosed volume.

2.4. Noncovalent Interactions by NCIPLOT Approach

To assess the nature of interactions in terms of being attractive or repulsive, we have used NCIPLOT, which is a novel software for plotting noncovalent interaction regions,[37a] based on the NCI (Noncovalent interactions) visualization index derived from the electron density.[37b] Reduced density gradient (RDG), derived from the electron density and its first derivative, is plotted (2D-plot) as a function of the density (mapped as isosurfaces) over the molecule of interest. The sign of the second Hessian eigenvalue times the electron density [i.e., sign(λ_2)ρ in atomic units] enables the identification of attractive/stabilizing (favorable) values identify the type of bonding, where large negative values specify attractive/stabilizing (favorable) hydrogen bonding, while large positive values specify repulsive (unfavorable) interactions. The weak van der Waals interactions are specified by the values of sign(λ_2)ρ near zero.

The isosurfaces are visualized employing the VMD (visual molecular dynamics) molecular graphics viewer,[38] while the 2D-plots are shown with GNUPLOT.[39] In the NCI-plots, the nature of the specific interactions is highlighted through a red-blue-green color scheme on the calculated isosurface. Strong attractive interaction is indicated in blue whereas red indicates strong repulsion. Weak interactions appear green on the isosurface.

2.5. Intermolecular Energies

For each crystal structure under consideration, intermolecular energies for molecular pairs were calculated using the CLP (Coulomb–London–Pauli) approach implemented in the PIXEL program package.[40] Accurate electron densities around the molecules were computed at MP2/6–31G** level using Gaussian16.[41]

Intermolecular interaction energies for specific molecular pairs were also computed using CrystalExplorer21.5,[35] by summing up four energy contributions, namely electrostatic (E_{ele}), polarization (E_{pol}), dispersion (E_{dis}), and exchange–repulsion (E_{rep}). The calculations were performed from the monomer wavefunction at the B3LYP/6–31G(d,p) energy model with scale factors to determine total energy E_{tot}: $k_{ele} = 1.057$, $k_{pol} = 0.740$, $k_{dis} = 0.871$, and $k_{rep} = 0.618$. A cluster of molecules within a radius of 3.8 Å for a central molecule was generated. The results include a color-coded molecular cluster related to the particular interaction energy. Pair-wise energies are represented graphically as framework energy diagrams, which are restricted to electrostatic and dispersion-energy terms, and total energies.[27] The energies are visualized as cylinders linking the centers of mass of the molecules, where the cylinder thickness is proportional to the magnitude of the interaction energy. The cylinders are red for the electrostatic term, green for dispersion term, and blue for total energy.

2.6. Computational Methods

The calculations of the intramolecular C—H···Ni interactions were carried out using Gaussian16[41] and the PBE0-D3/def2-TZVP level of theory.[42] For this purpose, the crystallographic coordinates have been used and only the position of the H-atoms were optimized. The quantum theory of "atoms in molecules" (QTAIM)[43] has been used to study the interactions discussed in this study by means of the Multiwfn program[44] and represented using the VMD visualization software.[38] The NCI-plot isosurfaces were also used.[37] The color scheme is red-yellow-green-blue scale with red and blue for repulsive and attractive interactions, respectively. The cubes needed to generate the NCI-plot surfaces were computed at the same level of theory using the wavefunctions generated by means of the Gaussian16 program. Further, the NBO analysis[45a] was performed using the same level of theory and the NBO7.0 program.[45b]

3. Results and Discussion

3.1. Molecular Structure of [$FeCl_2(PPh_3)_2$], [$CoX_2(PPh_3)_2$] (X = Cl, Br), [$NiX_2(PPh_3)_2$] (X = Cl, Br, I), [$ZnCl_2(PPh_3)_2$], and [$NiX_2(PBz_3)_2$] (X = Cl, Br)

Views of molecular structure of the series of seven M(II) (M = Fe, Co, Ni, Zn) dihalide-complexes with triphenylphosphine: a) GATXOP, b) BIHGEE, c) BIHGII, d) CLTPNI03, e) BPOLEX, f) ZZZKQO01, and g) GUXVAW, and two Ni(II) dihalide-complexes with tribenzylphosphine: a) XEGZIS and b) GAHLOR are shown in Figures 1 and 2, respectively.

Research Article
doi.org/10.1002/slct.202404665

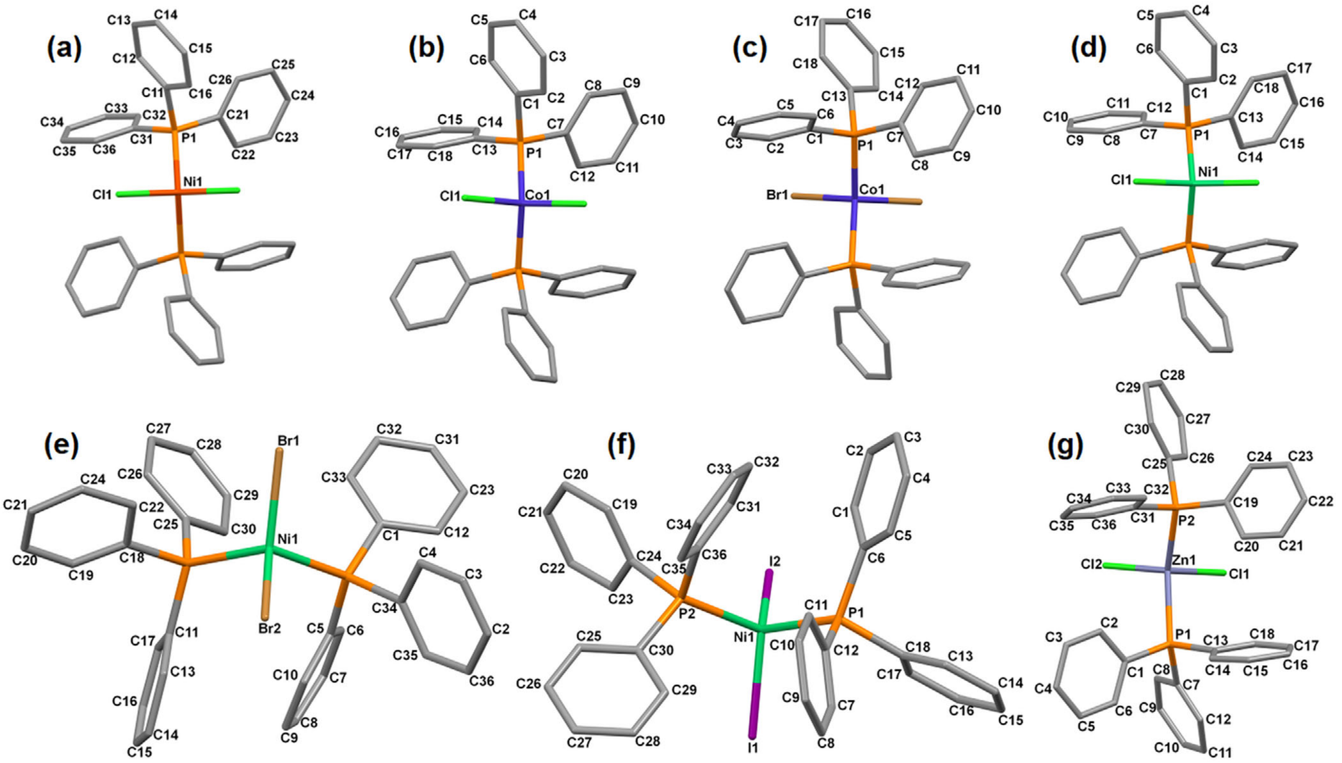

Figure 1. View of molecular structures of a) GATXOP, b) BIHGEE, c) BIHGII, d) CLTPNI03, e) BPOLEX, f) ZZZKQO01, and g) GUXVAW with the atom numbering scheme. H-bonds are omitted for clarity.

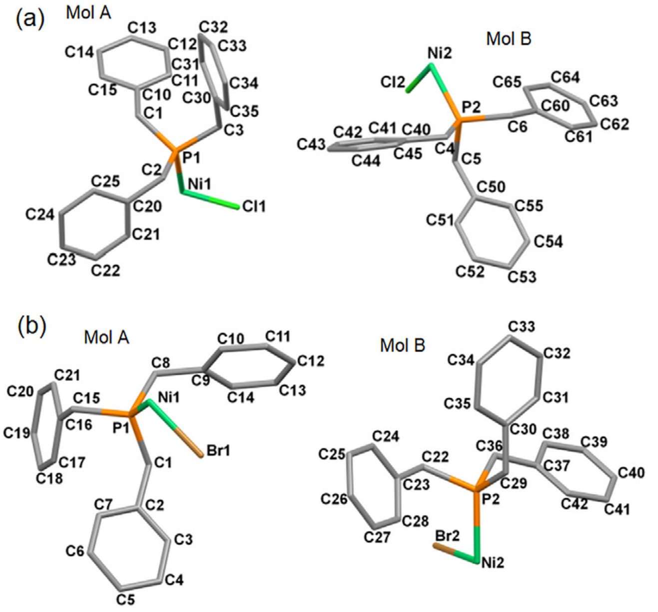

Figure 2. Molecular structures of a) XEGZIS and b) GAHLOR showing the asymmetric unit and the atom numbering scheme. H-bonds are omitted for clarity.

3.2. Analysis of Isostructurality

Some degree of similarity in the unit cell parameters with common space groups P2/c for GATXOP, BIHGEE, BIHGII and CLTPNI03, and $P\bar{1}$ for XEGZIS and GAHLOR can be seen in Table 1. Further, the similarity in the molecular packing is underscored by the similar unit-cell volumes, which is most evident for the pairs GATXOP/CLTPNI03, BIHGEE/BIHGII, and XEGZIS/GAHLOR. All these features suggest potential existence of isostructurality.

Firstly, we computed the unit-cell similarity index π in order to estimate the internal motion of the lattice parameters in the six pairs corresponding to the group of four complexes (rows 1–6, column 1, Table 2), and in the pair XEGZIS/GAHLOR. The calculations lead to values almost zero in the range 0.0018–0.0254, which indicate high lattice similarity.

For estimating the effect of the differences in the geometry of the molecules and the positional differences on the structural similarity, the isostructurality index $I_i(21)$ from the asymmetric unit as "isostructural core" of 21 pairs of nonhydrogen atoms for six pairs of triphenylphosphine-containing complexes (GATXOP, BIHGEE, BIHGII, and CLTPNI03) was computed (Table 2). In the pair of tribenzylphosphine-containing complexes (XEGZIS and GAHLOR), $I_i(24)$ from an "isostructural core" of 24 pairs of nonhydrogen atoms was calculated comparing separately the molecules A and B. The results reveal high isostructurality ($I_i > 80\%$) for all the pairs of structures, except for BIHGII/CLTPNI03 with $I_i = 79.2\%$.

The lowest π values of 0.0026 for GATXOP-BIHGEE and 0.0052 for BIHGEE-BIHGII are associated to shortest $I_i(21)$ percentages of 90.3 and 90.7, respectively, whereas the highest π values of 0.0254 for BIHGII-CLTPNI03 and 0.0203 for BIHGEE-CLTPNI03 are associated to longest $I_i(21)$ values of 79.2 and 82.5, respectively. However, an accurate correlation between π and $I_i(21)$ values was

Table 1. Crystal data of the seven dihalide-complexes with PPh_3 and the two Ni(II) dihalide-complexes with PBz_3.

	GATXOP	BIHGEE	BIHGII	CLTPNI03	BPOLEX	ZZZKQO01	XEGZIS	GAHLOR	GUXVAW
SG	P 2/c	P 2/c	P 2/c	P 2/c	P 21/n	P 21/c	P1	P1	P 21/c
a	11.7937(13)	11.764 (2)	11.828 (2)	11.580(2)	9.828(2)	19.361(17)	10.4892(15)	10.497(4)	11.816(7)
b	8.1652(9)	8.250 (3)	8.325 (2)	8.094(1)	37.178(9)	10.220(5)	10.5249(12)	10.538(4)	17.205(7)
c	17.0760(19)	17.254 (7)	17.365 (5)	17.220(3)	10.024(3)	17.995(13)	19.453(2)	19.556(9)	16.940(7)
α	90	90	90	90	90	90	83.872(8)	84.58(4)	90
β	106.202(2)	106.57 (4)	106.58 (3)	107.20(2)	114.65(2)	112.26(7)	76.839(9)	76.42(3)	104.55(4)
γ	90	90	90	90	90	90	62.241(8)	63.33(2)	90

Table 2. Unit-cell similarity index π, isostructurality index $I_i(n)$, degree of lattice distortion S, measure of similarity Δ, packing similarity PS$_{ab}$, and dissimilarity index X for pair of structures must closely packing.

	$\prod$	$I_i(n)$[a]	S	Δ	PS$_{ab}$	X		
						0D	2D	3D
GATXOP-BIHGEE	0.0026	90.3	0.0049	0.033	0.1603	–	–	7.7
GATXOP-BIHGII	0.0079	85.4	0.0087	0.040	0.1645	14.9	–	–
GATXOP-CLTPNI03	0.0177	86.0	0.0089	0.049	0.3257	–	1.8	–
BIHGEE-BIHGII	0.0052	90.7	0.0042	0.014	0.1484	–	1.8	–
BIHGEE-CLTPNI03	0.0203	82.5	0.0098	0.025	0.3234	–	1.7	–
BIHGII-CLTPNI03	0.0254	79.2	0.0125	0.023	0.3558	14.3	–	–
XEGZIS-GAHLOR	0.0018	90.7[b] 82.3[c]	0.0068	0.016	0.1460	–	1.6	–

[a] n is 21 y 24 for pairs with PPh_3 and PBz_3, respectively.
[b] Between molecules A.
[c] Between molecules B.

not observed. Hence, we have carried out the identification of atomic displacements that link pairwise the atomic positions in each pair of structures by means of the degree of lattice distortion (S) and the measure of similarity (Δ). These descriptors are considered in all situations where geometrical relationships between lattices or crystal structures have to be described, and the computed results are shown in Table 2.

It can be observed that the pair BIHGEE-BIHGII presents the shortest S (0.0042) value for the six pairs of dihalide-complexes with PPh_3, according to the highest isostructural similarity reflected by the $I_i(21)$ value (90.7%). This confirms that the crystal lattice and the geometry of molecules are unaffected by the nature of the halide for the two Co(II) complexes. By the other hand, the degree of lattice distortion is greatest for the pair BIHGII-CLTPNI03 ($S = 0.0125$) as obtained from the highest π (0.0254) and shortest $I_i(21)$ (79.2%) values, consistent to both the replacement of halide and metal ion.

Taking into account that the measure of similarity (Δ) does not correlate well with π and $I_i(21)$ values, we have calculated the packing similarity PS$_{ab}$ by using of CrystalCMP software. The similarities and differences in the molecular packing were analyzed employing a packing similarity tree diagram. The tree diagram is used for a better analysis of similarity in the crystal packing of a group of structures. The dendrogram and accompanying similarity matrix for the set of seven structures with triphenylphosphine are shown in Figure 3. Comparison were performed according to C1C(P(C)C)CCCC1 smiles atoms.

From the packing similarity dendrogram, we can identify two distinct "isostructural" families. The closest-packing family contains four structures (BIHGEE, BIHGII, GATXOP, and CLTPNI03) which are clustered at PS$_{ab}$ values from 0.1424 (BIHGEE-BIHGII) to 0.3312 (links shaded green), while a less close-packing family of five further structures (BIHGEE, BIHGII, CLTPNI03, GATXOP, and GUXVAW) are linked to the group with $5.9720 \leq$ PS$_{ab}$ ≤ 6.0871 (links shaded orange). It can be seen that a group containing CLTPNI03 GUXVAW, BPOLEX, and ZZZKQO01 shows dissimilar packing with PS$_{ab}$ between 16.5823 and 20.0633 (links shaded dark red). These surprisingly high PS$_{ab}$ values are not expected given the evident visual molecular similarity between pairs of structures belonging to this group, and could denote that corresponding molecules may not be adequately mapped.

The dendrogram and accompanying similarity matrix for the set of two structures with tribenzylphosphine are shown in Figure 3. Comparison was performed according to [Ni](P(CC)(CC)CC)—(P(CC)(CC)CC) smiles atoms. It can be observed that these structures (XEGZIS and GAHLOR) are clustered at PS$_{ab}$ value of 0.1460 (links shaded green), which reveals a very close-packing isostructural pair.

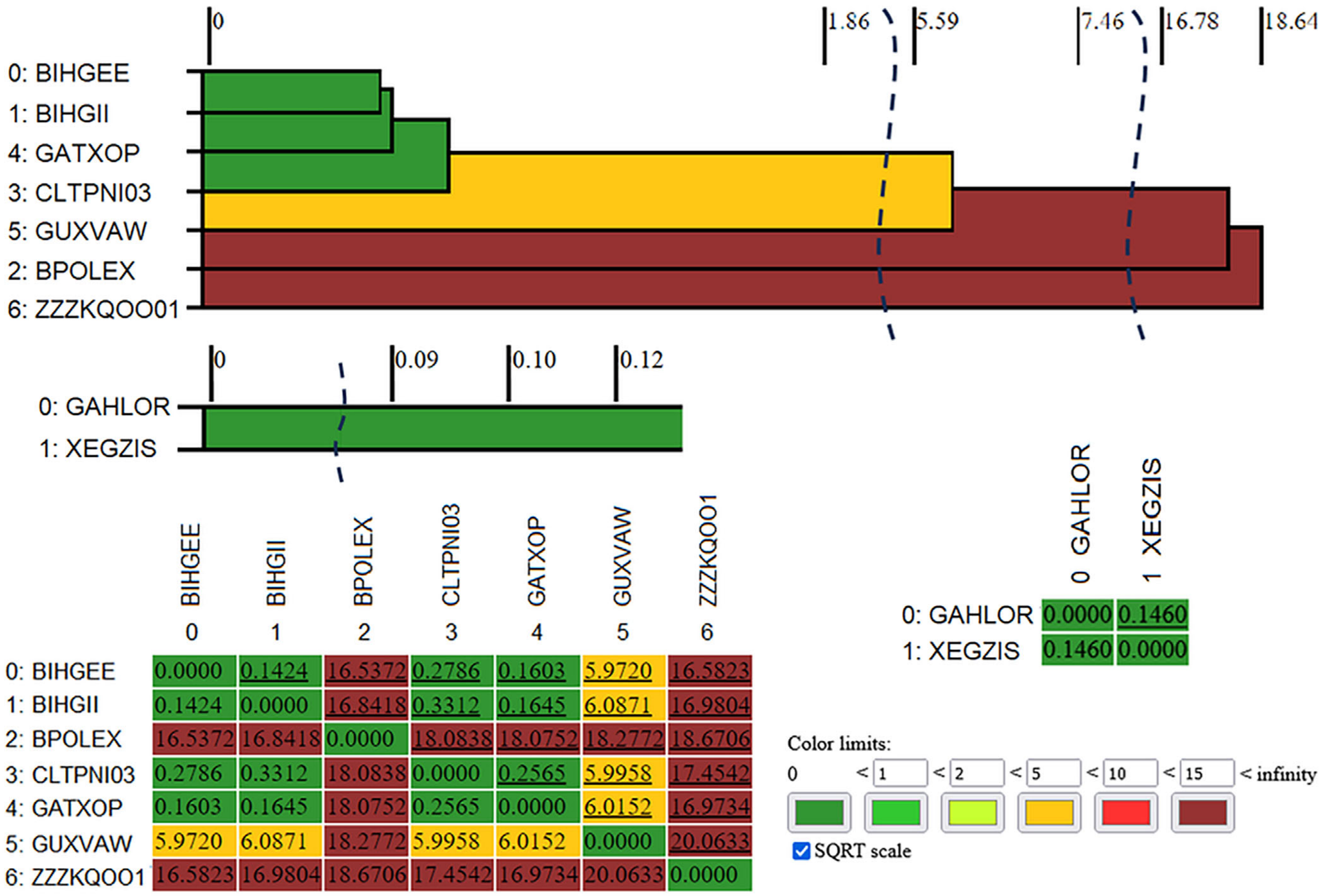

	0 BIHGEE	1 BIHGII	2 BPOLEX	3 CLTPNI03	4 GATXOP	5 GUXVAW	6 ZZZKQO01
0: BIHGEE	0.0000	0.1424	16.5372	0.2786	0.1603	5.9720	16.5823
1: BIHGII	0.1424	0.0000	16.8418	0.3312	0.1645	6.0871	16.9804
2: BPOLEX	16.5372	16.8418	0.0000	18.0838	18.0752	18.2772	18.6706
3: CLTPNI03	0.2786	0.3312	18.0838	0.0000	0.2565	5.9958	17.4542
4: GATXOP	0.1603	0.1645	18.0752	0.2565	0.0000	6.0152	16.9734
5: GUXVAW	5.9720	6.0871	18.2772	5.9958	6.0152	0.0000	20.0633
6: ZZZKQO01	16.5823	16.9804	18.6706	17.4542	16.9734	20.0633	0.0000

	0 GAHLOR	1 XEGZIS
0: GAHLOR	0.0000	0.1460
1: XEGZIS	0.1460	0.0000

Color limits:
0 < 1 < 2 < 5 < 10 < 15 < infinity
☑ SQRT scale

Figure 3. Dendrograms showing the packing similarity of dihalide-complexes with a) PPh_3 and b) PBz_3. The horizontal axis corresponds to the PS_{ab} value (similarity). Dark green indicates almost identical packing and dark red indicates dissimilar packing. Parts of the dendrogram between 1.86 and 5.59, and between 7.46 and 16.78 for (a), and between 0.0025 and 0.08 for (b) were removed to make the figures shorter; the vertical curved lines indicate this deletion.

With the aim to identify similar supramolecular constructs (SCs), which are subcomponents of a complete crystal structure (0, 1, or 2 dimensionalities), we have calculated the dissimilarity index "*X*" for the set of six pairs of dihalide-complexes with PPh_3, and the pair with PBz_3 (Figure S1, ESI†). The comparison of structures is based on relative geometric conformations and positions of molecules without any directional intermolecular interactions. The group of atoms corresponding to the asymmetric unit was used to define the COSP.[33] The analysis of all the seven structures with triphenylphosphine reveals occurrence of 3D SC only in case of GATXOP/BIHGEE (see Table 2), thus revealing isostructurality between these two structures.

The occurrence of 2D "supramolecular constructs" in the crystal packing for GATXOP/CLTPNI03, BIHGEE/BIHGII, and BIHGEE/CLTPNI03 reveals layer of molecules match with high structural similarity as reflected by low and similar *X* values around 1.8, in agreement with closest-packing we have obtained using CrystalCMP for this group of four complexes. The same supramolecular dimensionality is observed in the case of tribenzylphosphine complexes, where the *X* value of 1.6 indicates a high structural similarity of XEGZIS with GAHLOR. The stretch parameter *D* of 0.10 Å and the *X*(i) versus delta(*d*) and delta(*p*) versus delta(*a*) plots reveal in general a small extent of stretching in one structure compared to the other. Furthermore, the pairs of structures GATXOP/BIHGII and BIHGII/CLTPNI03 are based on a common discrete (zero-dimensional) building block 0D, particularly an H-bonded dimer, with similar *X* values of 14.9 and 14.3, respectively, as expected when both the halide and metal ion are substituted.

3.3. Steric Description of the Ligands

In order to measure the steric demand of ligands, the solid angle Ω (str), "exact" solid angle Ω° (deg), equivalent cone angle ECA (deg), "exact" cone angle $\theta°$ (deg) and G-parameters (%) of ligands, entire complex, and metal for all the nine complexes were calculated. The results listed in Table S1, ESI show longer "exact" cone angle $\theta°$ values than those of the idealized Tolman standard values of 145° (PPh_3)[5] and 165° (CH_2PPh_3)[6,46] for all the structures in agreement to the literature,[8] with mean absolute deviations of 9.3° and 21.1°, respectively.

In other systems with bulky ligands we have previously reported,[47] the cone angle decreases with the actual M-P distance increases.[8] However, a group of four Ni(II) complexes

(BPOLEX, ZZZKQO01, XEGZIS, and GAHLOR) and the Zn(II) complex (GUXVAW) show slightly internal mismatches for the two phosphine ligands in their cone angles, indicating no significant effect of the chemical environment on the steric bulk of each ligand.

In order to evaluate the probability of an incoming reagent not accessing the metal center, G(L), G(complex), and G(M) were computed from ligand solid angles Ω (Table S1, ESI). A solid-G view for all the complexes is shown in Figure S2, ESI highlighting the areas of the ligands projection shadow on a sphere of an arbitrary radius. As expected, the percentages of the sphere shielded by the PPh_3 ligand are in the range 23.6%–27.2%, which are longer than that for the halide ligand (15.3%–19.4%), and hence the remaining open area (white) of the sphere where an incoming reagent could bind represents a small percentage, varying from 8.4% in dibromide complex BPOLEX to 20.8% in dichloride complex GUXVAW.

The G(complex) values indicate that all the ligands shield from 78.5% (GATXOP) to 88.8% (BPOLEX) of the metal's coordination sphere. The highest G(M) value of 75.0% for BPOLEX denotes that there is only a 25.0% chance that an incoming reagent reaches the nickel center. In comparison to Co(II) dichloride-complex BIHGEE, the G(M) value is 7.2% longer than that of the dibromide homologous BIHGII, whereas the maximum percentage (Mol 1) of 74.0% for the dibromide Ni(II) complex GAHLOR is 4% higher than that for the dichloride homologous XEGZIS. These results indicate similar effect of halide-substituent variation on the steric hindrance in metal dihalide-complexes with PPh_3 and PBz_3.

In terms of the solid angle Ω, "exact" solid angle Ω°, equivalent cone angle (ECA), and "exact" cone angle $\theta°$ of PPh_3 ligand, the diiodide complex (ZZZKQO01) presents the lowest values (3.1°, 119.0°, 151.8°, and 24.7°), the dichloride complex (CLTPNI03) presents the intermediate values (3.3°, 123.5°, 156.5°, and 26.3°), and the dibromide complex(BPOLEX) presents the highest values (3.4°, 125.6°, 159.9°, and 27.2°). This order of variation is the same than the root-mean-square distortion (rmsd) of the angles at nickel from the tetrahedral ideal as reported in literature,[16] which supports the statement of differing intramolecular steric requirements of the PPh_3 ligand are at least partially responsible for the observed angles at nickel, as previously suggested by some authors.[17]

3.4. Intramolecular Anagostic Interactions in XEGZIS and GAHLOR

Considering that the hydrogen-atom positions determined by X-ray diffraction are unreliable because hydrogen has a low scattering power for X-rays, the aromatic C—H bond lengths from X-ray analysis (0.93 Å) in XEGZIS and GAHLOR were normalized to neutron hydrogen distance of 1.083 Å[48] using Olex2.[49]

Unlike the tetrahedral complexes with the bulky PPh_3 ligand, the packing effects together with the steric and electronic hindrance of both bulkier PBz_3 ligand in XEGZIS and GAHLOR, allow an aromatic *ortho*-proton of a Bz_3P group to be nearly close to one of the vacant positions around the nickel atom, with Ni1···H21 = 2.827(1)Å and C21—H21 · · · Ni1 = 113.9° (XEGZIS, Mol A), Ni2···H65 = 2.757(1) Å, and C65–H65· · ·Ni2 = 143.9° (XEGZIS, Mol B), whereas Ni1· · ·H10 = 2.850(2)Å and C10—H10 · · · Ni1 = 110.5° (GAHLOR, Mol A), Ni2···H28 = 2.804(1)Å, and C28—H28 · · · Ni2 = 142.9° (GAHLOR, Mol B). These rare interactions in which a hydrogen atom is held close to a metal centre M are termed as anagostic or preagostic interactions.[20]

The anagostic M···H—C interactions are characterized by relatively long M···H distances (2.3 to 2.9 Å) and large angles (110° to 170°), in comparison to agostic interactions which present relatively short M· · ·H distances (1.8 to 2.3 Å) and C—H···M angles ranging from 90° to 140°.[43] Complexes that contain anagostic interactions are square-planar, and they are typically associated with d^8 transition metals centers.[20] It can be observed that intramolecular Ni···H—C interactions for XEGZIS and GAHLOR are geometrically in the range of anagostic interactions.

These interactions are also distinguished by ^1H NMR spectroscopy, with NMR δ_H downfield shifts for uncoordinated C—H, in comparison to agostic interactions which are characterized by NMR δ_H upfield shifts.[43] Unlike the related triphenylphosphine-containing complexes, experimental ^1H NMR spectra of these two complexes with more sterically demanding phosphine ligand have not been reported at present, probably caused by the low yields in the synthesis, which hampers the NMR characterization.

It has been reported that the yield of the complexes decreases with increasing steric bulk of the ligand,[50] which is attributed to the increased steric bulk around the lone pair on the phosphorous atom, as the cone angle increases. This result helps to explain not only the high difficulty of coordination of the PPh_3 ligand to the metal center leading to side reactions, but also the small number of complexes reported with bulkier ligand as PBz_3. Thus, for example, the low yield that one of us obtained in the preparation of XEGZIS was associated to the collateral formation of tribenzylphosphine oxide crystals.[51]

To overcome these experimental hindrances, we have simulated the ^1H NMR spectra for XEGZIS and GAHLOR from their respective crystal structures (Figure S3, ESI†), using Gaussian16, SCF GIAO method, 6–311 + G(2d,p) basis set with the B3LYP functional, and tetramethylsilane (TMS) as reference.[41] A 6–31G* basis was used for H, C, P, and Cl atoms, while Ni atom was described by the LANL2DZ basis. Geometry optimization was performed using the mPW1PW91/SDD method.[52] Overlay diagrams of the crystal structure (showing atomic identities) over the optimized structure for XEGZIS and GAHLOR is depicted in Figure S3, ESI†. The degree of similarity between the superimposed molecules is more visible in XEGZIS, as reflected by the alignment RMSD values of 0.959 Å and 1.847 Å for molecules A and B, respectively, in comparison with the corresponding values of 1.381 Å and 2.043 Å for GAHLOR.[46]

As shown by the selected experimental and optimized parameters in Table S2, ESI, the basic experimental geometry (bond lengths and bond angles) was withheld in the optimized

Table 3. Interaction energies (E_{tot}) partitioned into coulombic, polarization, dispersion, and repulsion contributions (KJ/mol) for all the nine complexes.

M	X	Compound	Symmetry	Involved Interactions	H·· ·*Cg*/X ∠C-H···X	R	E_{coul}	E_{pol}	E_{disp}	E_{rep}	E_{tot}
Dihalide-bis(triphenylphosphine)M(II)											
Fe	Cl	GATXOP	–x,1-y,-z	C35-H35·· ·*Cg*2, C34-H34·· ·Cl1	2.854 2.943119	8.57	−43.7	−17.0	−79.6	46.8	−89.3
Co	Cl	BIHGEE	1-x,1-y,-z	C16-H16·· ·Cl1, C17-H17·· ·*Cg*2	2.978120	8.64	−42.6	−16.2	−73.1	37.1	−89.8
	Br	BIHGII	$x,-y,-\frac{1}{2}+z$	C3-H3·· ·*Cg*2	2.898	8.78	−38.2	−12.9	−77.2	41.3	−83.5
			$1+x,-y,\frac{1}{2}+z$	C17-H17·· ·*Cg*1	2.932	8.33	−19.7	−15.8	−66.4	34.5	−62.2
Ni	Cl	CLTPNI03	$x,1-y,-\frac{1}{2}+z$	C9-H9·· ·*Cg*3, C9-H9·· ·Cl1	2.778 2.916118	8.64	−45.5	−17.6	−82.4	51.8	−90.0
	Br	BPOLEX	–x,-y,-z	C3-H3·· ·*Cg*1	2.917	10.19	−21.4	−3.7	−74.4	38.7	−59.8
	I	ZZZKQO01	$x,\frac{1}{2}-y,\frac{1}{2}+z$	C16-H14·· ·*Cg*5, C15-H13·· ·I1	2.701 3.131135	9.45	−22.4	−8.3	−50.3	19.0	−58.2
			x,-1 + y,z	C33-H28·· ·I2, C10-H9·· ·I1	3.309132 3.382129	10.22	−17.3	−8.1	−33.3	20.1	−36.7
Zn	Cl	GUXVAW	$x,\frac{1}{2}-y,-\frac{1}{2}+z$	C3-H2·· ·Cl1, C35-H29·· ·Cl1, C17-H14·· ·Cl2	2.733159 2.917121 2.820125	8.47	−48.1	−19.5	−67.7	41.8	−88.9
			$2-x,-\frac{1}{2}+y,\frac{1}{2}-z$	C33-H27·· · Cl2	2.714145	9.94	−17.3	−9.1	−37.8	22.8	−39.1
			$1+x,\frac{1}{2}+y,\frac{1}{2}+z$	C11-H9·· ·*Cg*6	2.922	12.69	−2.6	−1.7	−31.6	0.0	−32.2
Dihalide-bis(tribenzylphosphine)M(II)											
Ni	Cl	XEGZIS	−1-x,-y,-z	C15-H15A··· *Cg*3, C25-H25A·· ·*Cg*1	2.513 2.699	10.49	−27.6	−4.4	−109.7	72.7	−83.0
			−1 + x,y,z	C64-H64A·· ·*Cg*5	2.853	9.73	−18.4	−4.0	−65.2	43.1	−52.6
	Br	GAHLOR	1-x,-y,-z	C3-H3·· ·*Cg*3, C14-H14·· · *Cg*1	2.522 2.733	10.50	−8.8	−6.7	−82.2	34.6	−59.3
			1-x,-y,1-z	C27-H27·· · *Cg*5	2.882	10.50	−32.4	−9.0	−111.6	56.4	−93.6
			−1 + x,y,z	C11-H11·· · *Cg*4	2.941	9.78	−21.3	−6.6	−65.8	33.2	−58.4
			x,y,-1 + z	C19-H19·· · *Cg*6	2.950	10.50	−8.8	−6.7	−82.2	34.6	−59.3

[a] *Cg*2 is the centroid of C21—C26 and C7—C12 rings for GATXOP and BIHGEE, respectively; *Cg*1 and *Cg*2 are the centroids of C1—C6 and C7—C12 rings for BIHGII; *Cg*5 is the centroid of C25—C30 for ZZZKQO01; *Cg*2 and *Cg*3 are the centroids of C7—C12 and C13—C18 rings for CLTPNI03; *Cg*1 is the centroid of C1—C12—C23/C31—C33 ring for BPOLEX; *Cg*6 is the centroid of C31—C36 ring for GUXVAW; *Cg*1, *Cg*3, and *Cg*5 are the centroids of C10—C15, C30—C35, and C50—C55 for XEGZIS, respectively; *Cg*1, *Cg*3, *Cg*4, *Cg*5, and *Cg*6 are the centroids of C2—C7, C16—C21, C23—C28, C30—C35, and C37—C42 rings for GAHLOR, respectively.

structures for both complexes, with small average differences of 0.040 Å and 4.57°. However, the variations of 0.108 Å and 0.106 Å are notably longer in the case of d(Ni···H_{ortho}) distances involved in Ni···H—C anagostic interactions. Thus, the optimized Ni1···H21 and Ni1···H10 distances of 2.935 and 2.957 Å for molecule A of XEGZIS and GAHLOR, respectively, are slightly longer than the limit of anagostic contacts, mainly due to significant differences in the twist of the phenyl rings around the H_2C—C bond as shown by the P—C—C—C torsion angles. This prompted us to simulate the ^1H NMR spectra from the experimental structures as shown in Figure S4, ESI. The chemical shifts for all the 42 protons of each equivalent molecule are shown in Table S3, ESI. The H-atoms labeled 36, 134, 80, and 178 by GaussView for XEGZIS correspond to *ortho*-protons labeled 21, 21A, 65, and 65A in Figure 2a, whereas the H-atoms labeled 57, 143, 78, 1 and 64 for GAHLOR are related to 10, 10A, 28, and 28A *ortho*-protons in Figure 2b.

Compared to the remaining protons, it is clearly observed that the four protons abovementioned for each complex present the largest downfield shift (more deshielded), resonating in the ranges 6.18–6.85 ppm and 8.72–9.14 ppm for XEGZIS and GAHLOR, respectively, which suggest that all the eight protons are in close proximity to the nickel center. A comparison between molecules at x,y,z (Mol1) and between molecules at −x,−y,−z (Mol2) indicates that Ni1···H21—C21 and Ni2···H65—C65 of XEGZIS exhibit the strongest anagostic interactions as reflected by the largest downfield shift and shortest Ni···H distances. Remarkable downfield shifts for the *ortho*-protons of phenyl groups of tribenzylphosphine ligand are also observed in XEGZIS and GAHLOR as compared to its precursor ligand (refcode RILPUZ).[53] The H-atoms labeled 6, 14, 20, 28, 34, and 42 by GaussView6.0 for RILPUZ corresponding to *ortho*-protons labeled 3, 7, 10, 14,17, and 21 in the molecular structure, show δ_H shifts in the range 4.55–4.74 ppm (Table S2, ESI), which are shorter (less deshielded) than those of six *meta/para*-protons (4.80–4.90 ppm) of the phenyl rings. Hence, our analysis of predicted ^{1}H NMR spectra from X-ray data confirms the geometric results about the presence of anagostic interactions in the two tribenzylphosphine-containing complexes.

3.5. Noncovalent Interaction Analysis

We have observed that the description of intermolecular interactions is omitted by the original authors in papers of the three Ni(II) complexes (CLTPNI03, BPOLEX, and ZZZKQO01), the two Co(II) complexes (BIHGEE and BIHGII), and the Zn(II) complex (GUXVAW), whereas only the shortest intermolecular C16—H16···Cl1 contact is reported in GATXOP. Studies on intermolecular interactions are also absence for the two Ni(II) dihalide-complexes with PBz_3 (XEGZIS and GAHLOR), in the former only highlighting that the molecules in the crystal are packed at normal van der Walls forces.

This prompted the present study in which we perform a complete analysis of the noncovalent interactions, starting with the calculation of geometric parameters characterizing such contacts, which are evident in the output from PLATON program.[54] However, it is known that the application of atom–atom distance criteria based on sums of van der Waals radii is not enough to define the existence of an interaction.[55] That is why we have also performed energetic and surface analysis, noncovalent interaction plots, and crystal void analysis, which are tools currently used to complement studies on molecular and crystal packing.

We have found that the supramolecular assembly of all the nine complexes is characterized by the formation of dimers involving point-to-face C—H···π contacts[56] and weak C—H···X (X = Cl, Br, and I) hydrogen bonds.[57] In comparison with the seven dihalide-complexes with PPh_3, a more extensive network of the mentioned contacts is observed for XEGXIS and GAHLOR. Geometry of the interactions is shown in Table 3 (column 5).

Pixel energies partitioned into coulombic, polarization, dispersion, and repulsion contributions, in molecular pairs involving C—H···π and C—H···X interactions extracted from the crystal packing for six complexes are listed in Table 3. The energetic values show that the higher contribution towards the total crystal stabilization comes from the dispersion energy, representing similar percentages of 59.8, 59.9, 59.2, 58.6, 55.0, and 54.2 of cohesive energy in dimers corresponding to CLTPNI03, BPOLEX, GATXOP, BIHGEE, BIHGII, and GUXVAW, respectively. A detailed analysis of the total energies E_{tot} is discussed in energy frameworks section.

3.6. Hirshfeld Surface Calculations

Hirshfeld surface analysis have been carried out in order to get a better comprehension on the nature of C—H···π interactions in all the complexes studied.The donor and the acceptors of intermolecular C—H···π contacts can be recognized as blue and red regions around the participating atoms on the Hirshfeld surfaces mapped over shape-index property. The evidence of C—H···π/π···H—C contacts in all the nine structures is particularly clear with the presence of a large red depression (hollow) above the π-electron system and a large blue region (bump) surrounding the C—H donor as shown in Figure S5, ESI.

3.7. Reduced Density Gradient and Noncovalent Interaction Plots

To get a deeper insight into noncovalent intermolecular C—H···π interactions, we have calculated the reduced density gradient (RDG-plots) and noncovalent interaction isosurfaces (NCI-plots) for all the nine complexes. The plots have been computed from appropriated molecular fragments in order to analyze isolated H···π motifs (Figures 4 and 5). Distinct green spikes can be observed in the negative region of sign(λ_2)ρ (hereafter S), which are related to the strength of intermolecular interactions. The RDG plots for the seven M(II) complexes with PPh_3 (a, b c, d, e, f, g) show a unique spike with *S* value around −0.015 a.u., which is associated to C—H···π interactions (Figure 4). Two spikes are observed in the Ni(II) complexes with PBz_3 (Figure 5), one of them attributed to the strongest C—H···π interaction, characterized by a spike with *S* values around −0.025 and −0.020 a.u. for XEGZIS (H15A···*Cg*3 = 2.513 Å, Figure 5a) and GAHLOR (H3···*Cg*3 = 2.522 Å, Figure 5b), respectively, when compared with the corresponding weaker van der Waals interactions from H14A (3.870 Å) and H4 atoms (3.817 Å), which show a spike with *S* value around −0.010 a.u for both the complexes.

The green isosurfaces in the NCI-plots indicate H···*Cg* weakly attractive interactions, being largest for the strongest interaction in each complex. The red spike in the range 0.09–0.15 a.u. of RDG-plots corresponds to the steric effect within the benzene rings, being remarkably stronger for XEGZIS (S = 0.11 a.u.) in comparison with the remaining complexes.

The default range of *X*-axis of the plotting script was extended from −0.20 to 0.15 for XEGZIS and GAHLOR in order to show the corresponding chemical bond region, which is clearly revealed by a pair of blue spikes with *S* values between −0.19 and −0.17 a.u., confirming that electron density in these regions is very large and implying bonding effect is strong.

3.8. Crystal Voids

In order to assessing mechanical stability of the packed crystals, a void analysis was carried out. It is well-known that the crystal structures with large empty spaces show molecules which are not tightly packed, and hence they can be easily bro-

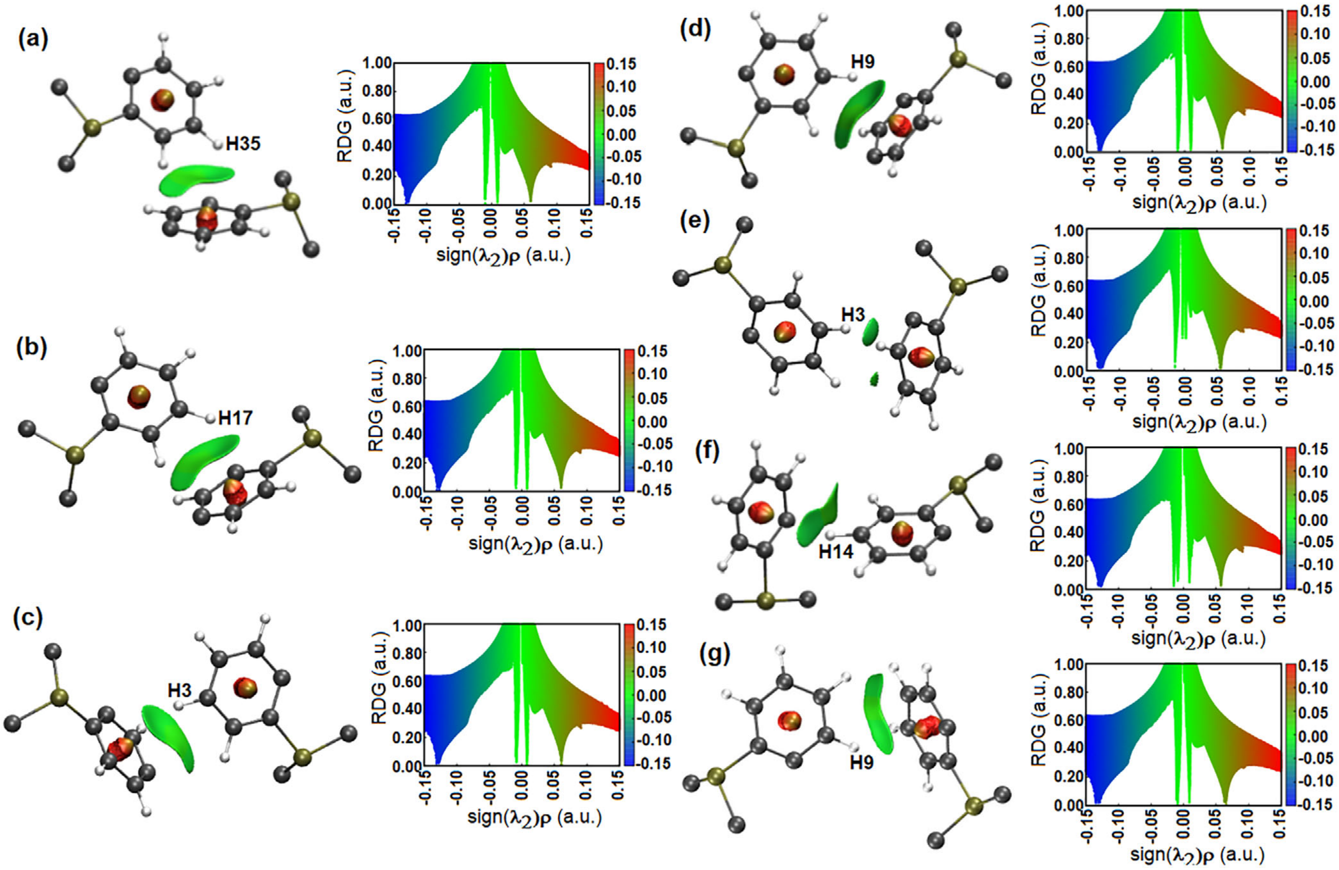

Figure 4. RDG plots and NCI isosurfaces (isovalue 0.050) of strongest C—H⋯π interactions for a) GATXOP, b) BIHGEE, c) BIHGII, d) CLTPNI03, e) BPOLEX, f) ZZZKQO01, and g) GUXVAW.

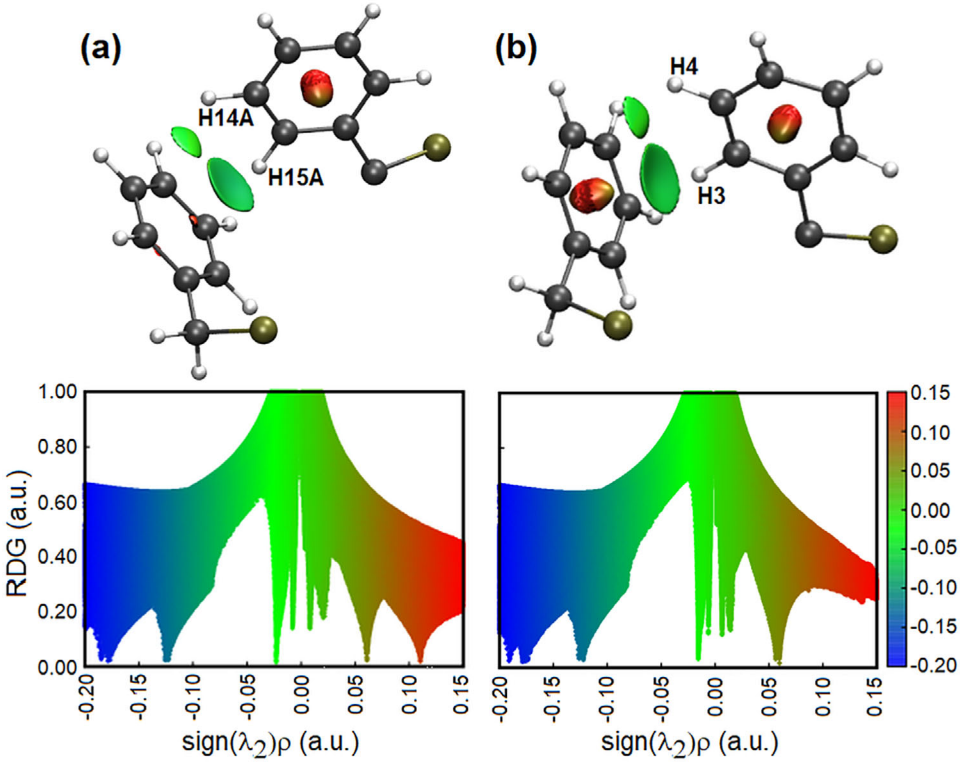

Figure 5. RDG plots and NCI isosurfaces (isovalue 0.050) of strongest C—H⋯π interactions for a) XEGZIS and b) GAHLOR.

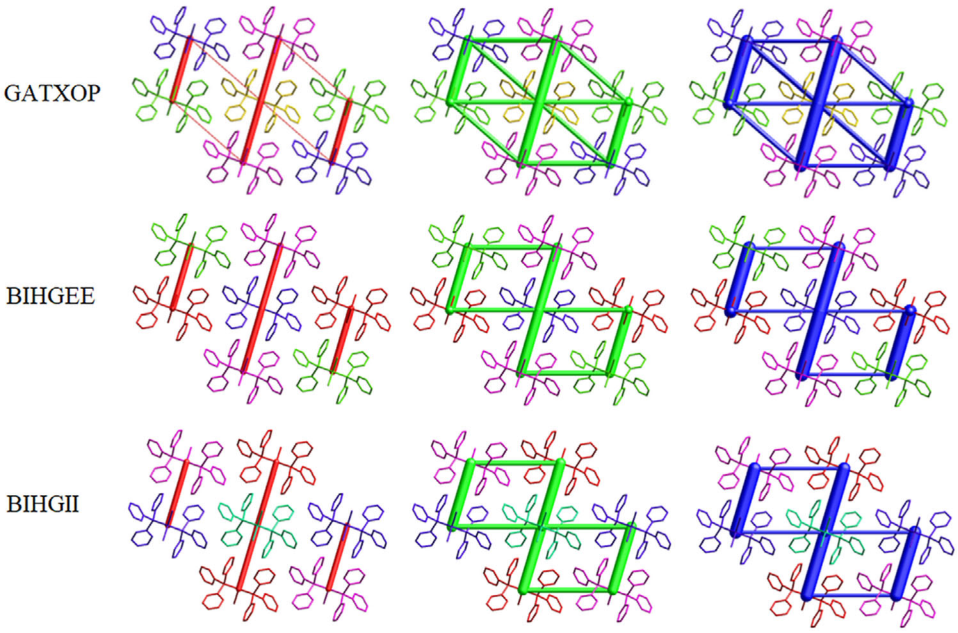

Figure 6. Energy frameworks of GATXOP, BIHGEE, and BIHGII viewed along *b*-axis direction for separate electrostatic (red) and dispersion (green) contributions to the total pairwise interaction energies (blue); H-atoms have been omitted for clarity; energy cylinder scale of 95, and energy threshold of 5.0 kJ/mol within 3 × 3 × 3 unit cells are the same in all nine diagrams, and for the next two figures.

ken provided small amount of external force is applied to the crystal.[39b] Voids in the crystal structure of our complexes have been calculated and visualized by creating (0.002 au) isosurface of procrystal electron density (Table S4, ESI; Figure S6, ESI). Crystal void volumes below 570.75 Å^3 associated with small % of free spaces in unit cell between 11% and 17% are indicative of any large cavity within the packed crystal, and hence the mechanical stability can be considered notable at room temperature for all the nine complexes.

Moreover, the isosurfaces are not completely closed around all the molecules but are open in the regions where noncovalent interactions occur. Considering both that the atomic radius of Fe is greater by 0.03 Å than that of Zn, and the similar molecular conformation in GATXOP and GUXVAW, the molecules for the former occupy more space in the unit cell, and hence the void volume decreases from 570.75 Å^3 in GUXVAW to 191.04 Å^3 in GATXOP.

3.9. Energy Frameworks

To better understand the 3D topology of the overall interaction energies between the molecules of a crystal in the systems under investigation, we have applied a method analogous to the PIXEL approach, using a CE–B3LYP/6–31G(d,p) energy model available in CrystalExplorer21.5,[25] thus enabling the calculation of intermolecular interaction energies in complexes ZZZKQO01, XEGZIS, and GAHLOR where the PIXEL method could not be applicable.

Intermolecular C—H$\cdots\pi$ contacts and C—H$\cdots$X (X = Cl and Br) hydrogen bond interactions are graphically represented as energy frameworks in Figure 6 (GATXOP, BIHGEE, and BIHGII), Figure 7 (CLTPNI03, BPOLEX, ZZZKQO01, and GUXVAW), and Figure 8 (XEGZIS, GAHLOR) from a list of intermolecular energies (Table S5, ESI). All the structures are characterized by a dominant dispersion energy framework followed by an electrostatic energy framework contribution as reflected by the thickness of cylinders. In complexes GATXOP, BIHGEE, and BIHGII, the C—H$\cdots\pi$ and H$\cdots$X (X = Cl and Br) contacts are represented as cylinders with similar thickness in a dimer chain of molecules occurring in a zig-zag fashion along the *b*-axis for GATXOP and BIHGEE, and along the diagonal of the *bc*-plane for BIHGII. These interactions contribute to stabilization with energies of − 89.3 kJ/mol, −88.4 kJ/mol, and −84.1 kJ/mol, respectively, in agreement with the corresponding pixel energies of −84.5 kJ/mol, 86.6 kJ/mol, and 86.4 kJ/mol (Table 3).

In contrast with the Co(II) complexes, the topology of the energy frameworks shows remarkable dissimilarity for the Ni(II) complexes with PPh$_3$ (Figure 7), where the strength and directionality of the C—H$\cdots\pi$ and H$\cdots$X interactions are much more sensitive to the nature of halogen atom. Those interactions are involved in the same dimer and contribute to crystal packing stabilization with energies of −90.0 kJ/mol and −57.5 kJ/mol for dichloride-complex (CLTPNI03) and diiodide-complex (ZZZKQO01), respectively. The energetic comparison with the bromo-complex (BPOLEX) is not performed due to the mentioned interactions participate in different dimers. However, it can be seen a more extensive network of interactions in BPOLEX when compared to the other two related Ni(II) complexes.

In Zn(II) dichloride-complex (GUXVAW) the C—H$\cdots\pi$ and H$\cdots$Cl interactions are involved in the same dimer $(x,\frac{1}{2}-y,-\frac{1}{2}+z)$, providing a high energy contribution of −88.9 kJ/mol towards the crystal packing, in agreement with the pixel energy of −90.8 kJ/mol.

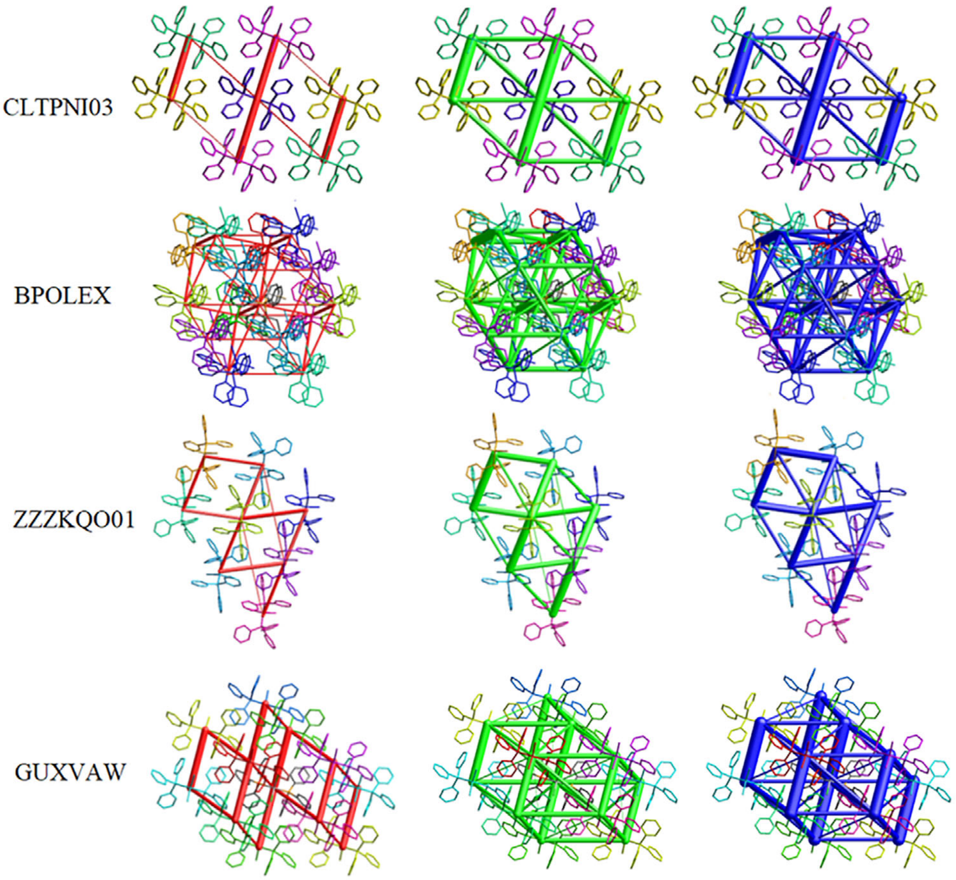

Figure 7. Energy frameworks of CLTPNI03, BPOLEX, ZZZKQO01, and GUXVAW viewed along *b*-axis direction for separate electrostatic (red) and dispersion (green) contributions to the total pairwise interaction energies (blue). H-atoms have been omitted for clarity.

Although a different topology of the energy frameworks is observed for XEGZIS and GAHLOR, an important common feature is the similar energetic contribution of the molecular pairs with shortest C—H···π interactions. Thus, the dimers involving C15—H15···Cg3 and C25—H25···Cg1 (−1−x,−y,−z) contacts (intercentroid distance $R = 10.49$ Å) for XEGZIS, and C3—H3···*C*g3 and C14—H14···*C*g1 (1−x,−y,−z) contacts (intercentroid distance $R = 10.50$ Å) for GAHLOR, present the highest energy contributions of −92.2 kJ/mol and −93.6 kJ/mol, respectively, in correspondence with the similar cylinder thickness. Further, these dimers are similarly stacked along the *b*-axis for both structures. By the other hand, the dimers involving C5—H5···Br1A hydrogen bonds (intercentroid distance $R = 11.04$ Å) in GAHLOR are stacked along *b*-axis, and provide an energy contribution of −31.8 kJ/mol towards the crystal packing, whereas intermolecular C23—H23···Cl2 (intercentroid distance $R = 9.73$ Å) in XEGZIS forms dimers stacked along *a*-axis with higher energy contribution of −60.2 kJ/mol due to the participation of C22—H22···*C*g6 contacts (see Table 3).

3.10. Theoretical Study of C—H···Ni Interaction in XEGZIS

In order to deduce the nature of the C—H···Ni interactions, we have firstly used the QTAIM theory for the molecule A of XEGZIS. These interactions could be purely electrostatic (with just penetration of van der Waals radii), covalent or partially covalent. In QTAIM theory, every chemical bond is characterized by a bond critical point (BCP) and a bond path interconnecting the atoms involved in the interaction. The BCP topology is described by the electron density (ρ), the Laplacian of electron density ($\nabla^2\rho$), the electronic kinetic (*G*), and electronic potential (*V*) energy density.

Figure 9 shows the QTAIM analysis for XEGZIS complex. In this structure, the C21—H21···Ni1 contact is characterized by a bond CP and a bond path that connects the phenyl *ortho*-H21 and the Ni(II) metal center. For this contact, the electron density (ρ) at the bond CP was 0.0072 a.u. This value is smaller than those reported for intramolecular X—H···M (X = C and N) interactions in d^8 square-planar complexes.[58] The positive value of the Laplacian of electron density ($\nabla^2\rho$) is associated with a closed-shell interaction, with an important electrostatic contribution.[58] In the same way, the positive value of the total energy density (H) is an indicator for purely closed-shell interaction.[59] In accordance with the formula proposed by Espinosa and coworkers ($E = \frac{1}{2}V$),[60] the energy associated to C21—H21···Ni1 is −1.38 kcal/mol, thus indicating that the H···Ni contacts are considered as very weak interactions, in comparison with classical hydrogen bonds. The NCI-plot of the complex shows a green isosurface located between the H21 and Ni1 atoms,

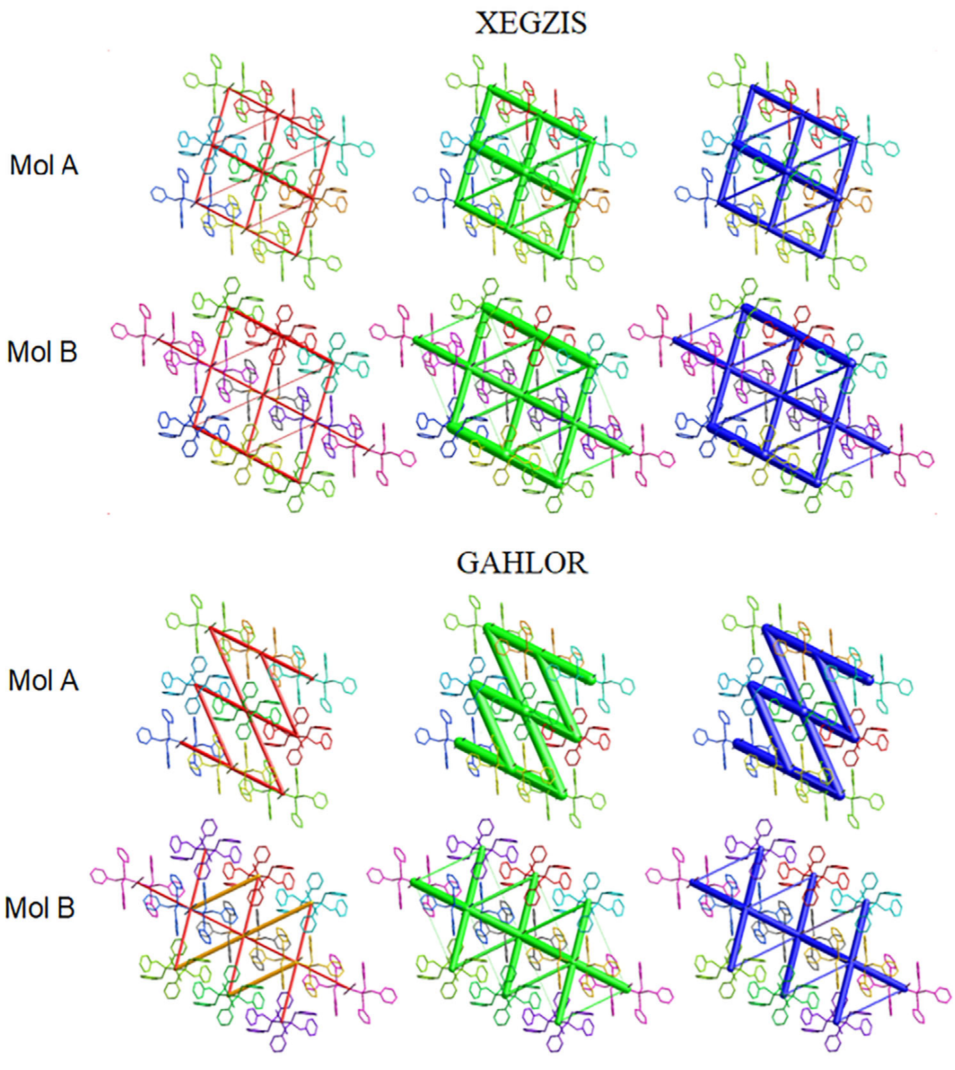

Figure 8. Energy frameworks of XEGZIS (top) and GAHLOR (bottom) viewed along *c*-axis direction for separate electrostatic (red) and dispersion (green) contributions to the total pairwise interaction energies (blue); Molecules A (above) and B (below). H-atoms have been omitted for clarity.

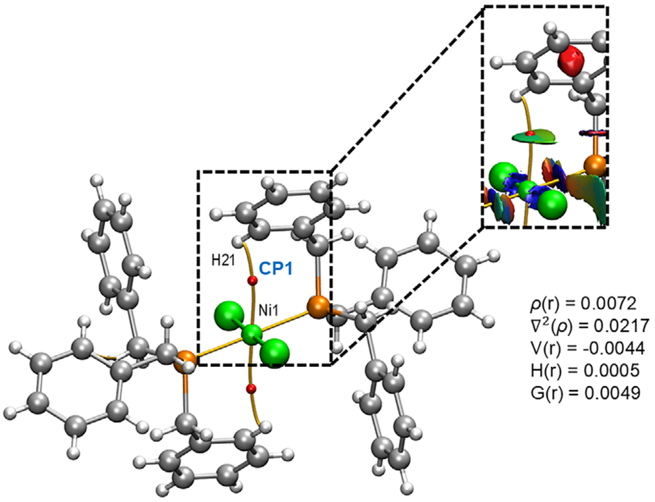

Figure 9. QTAIM analysis for molecule A of XEGZIS showing bond critical points (red spheres) and bond paths (orange lines) for the anagostic C21—H21···Ni1 interaction. Inset: NCI-plot diagram.

confirming the attractive nature of the anagostic C21—H21···Ni1 interaction.

Although the long Ni···H_{ortho} distances (2.757–2.850 Å) and the predicted ^{1}H NMR spectra suggest the presence of purely anagostic interactions for XEGZIS and GAHLOR, the low directionality of these contacts, as indicated by the short C—H···Ni bond angles ranging from 110.5° to 143.9°, could also hint at the existence of agostic interactions (90° $<$ C—H···Ni $<$ 140°). This observation prompted us to perform additional high-level theoretical calculations to further investigate the nature of these contacts. Specifically, we reanalyzed the C21—H21···Ni1 interaction in molecule A of XEGZIS, which features a very short C—H···Ni bond angle of 113.9°.

To differentiate between agostic interactions, where the σ(C—H) bond acts as an electron donor and the metal center as an electron acceptor, and anagostic interactions, where the metal center serves as the electron donor, we plotted electron density (ED) versus electrostatic potential (ESP) values along the bond path connecting the Ni atom

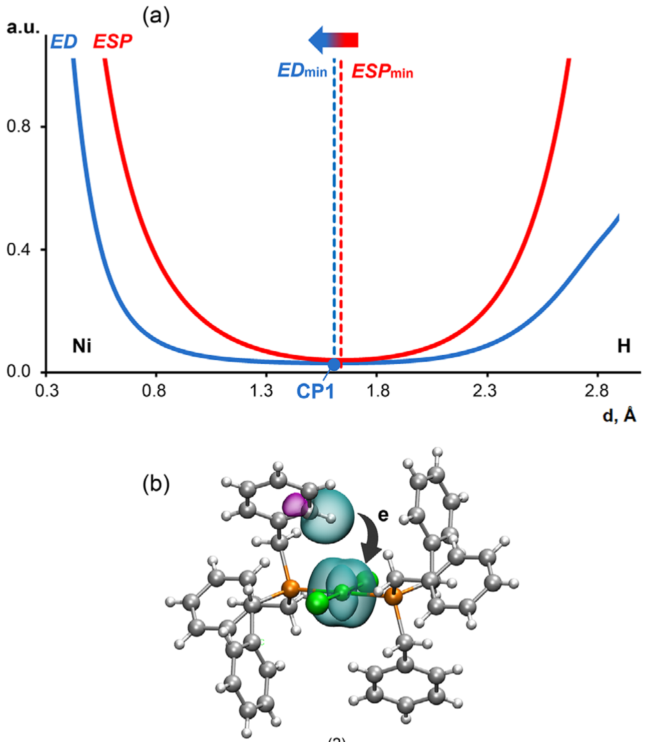

σ(C–H)→4s(Ni), $E^{(2)}$ = 0.28 kcal/mol

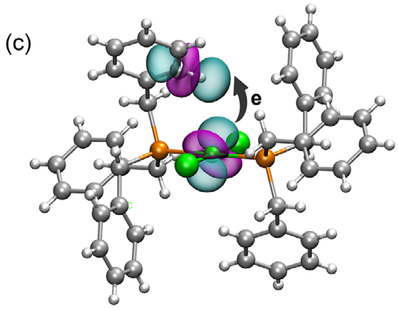

LP(Ni)→σ*(C–H), $E^{(2)}$ = 0.05 kcal/mol

Figure 10. (a) ED versus ESP plot computed for the bond path connecting the H to the Ni atom, as represented in Figure 10. (b) Plot of the NBOs involved in the σ(C—H) → 4s(Ni) donation. (c) Plot of the NBOs involved in the LP(Ni) → σ^*(C—H) donation. The second order perturbation energies are indicated.

to the H atom. It has been shown that the minimum electron density along this path is closer to the electron donor, while the minimum ESP is closer to the electron acceptor.[61] This approach proves useful in investigating donor–acceptor interactions.

Figure 10a presents the plot, showing that the positions of both minima are close to each other. A closer examination reveals that the ESP minimum is slightly nearer to the H atom, suggesting electron flow from the H atom to the Ni metal center, consistent with an agostic interaction.

Given the small distance between the ED and ESP minima, we further analyzed the interaction using NBO analysis, a method effective for studying noncovalent interactions from an orbital perspective.

Figure 10 displays two contributions: one supporting an agostic interaction (Figure 10b) and the other an anagostic interaction (Figure 10c). The NBO analysis indicates electron donation from the bonding σ(C—H) orbital to the empty 4s orbital of Ni(II), along with back-donation from a lone pair (LP) on Ni, located in the $d_{x^2-y^2}$ orbital, to the antibonding σ^*(C—H) orbital. The second-order perturbation energy for the σ(C—H) → 4s(Ni) donation is higher (0.28 kcal/mol) than the LP(Ni) → σ^*(C—H) back-donation energy (0.05 kcal/mol). Although both energy values are relatively small, the NBO analysis suggests a dominant agostic contribution, aligning with the ED versus ESP plot. To the best of our knowledge, no studies have been reported in the literature addressing the combined presence of both agostic and anagostic interactions.

4. Conclusions

This study presents a detailed structural and energetic analysis of nine metal phosphine dihalide complexes, providing significant insights into their stability and the role of noncovalent interactions in determining their structural integrity. The findings shed light on the ready dissociation commonly observed in these complexes, which has limited their pharmacological potential. By elucidating the influence of steric and electronic effects of the ligands, this work offers strategies to mitigate dissociation, thereby enhancing their suitability as pharmacological agents. Furthermore, the insights gained from this study hold considerable implications for ligand design in catalytic C—H bond functionalization. The understanding of ligand–metal interactions, steric constraints, and noncovalent contributions provides a framework for designing ligands that optimize reactivity and selectivity in catalytic systems. By bridging the gap between structural analysis and practical applications, this work emphasizes the dual utility of these complexes in medicinal chemistry and catalysis.

A deep investigation of the crystal structures revealed the existence of rare intramolecular Ni···H—C anagostic interactions for complexes with PBz_3, which were confirmed by ^{1}H NMR spectra. The crystal packing is stabilized by weak C—H···π interactions and C—H···X (Cl, Br, and I) hydrogen bonds. Shape-index surfaces, calculation of pixel energies, energy frameworks, reduced density gradient, and noncovalent interaction isosurfaces were used tools in describing the molecular packing, complementing the geometric analysis provided by PLATON. Crystal voids analysis indicated the mechanical stability of all the packed crystals, due to the absence of any large cavity. The theoretical analysis of the molecule A of XEGZIS complex reveals that the C21—H21···N1i interaction, as characterized by QTAIM and NBO analyses, are predominantly weak and electrostatic in nature, with a closed-shell character. The QTAIM results, supported by a low electron density at the bond critical point and a positive Laplacian of electron density, suggest an anagostic interaction. However, further examination using electron density versus electrostatic potential plots and NBO analysis indicates the presence of both agostic and anagostic contributions. Despite the weak interaction energies, the agostic interaction, characterized by electron donation from the C—H bond to the Ni metal center, appears to be dominant.

Supporting Information

Figures S1–S6 and Tables S1–S4

Acknowledgments

A. F. and R. G. M. acknowledge the financial support by the MICIU/AEI of Spain (projects PID2020-115637GB-I00 and PID2023-148453NB-I00, FEDER funds). D. M. G. would like to thank the SCAIT-UNT (Project D728), CONICET (PIP 215), and ANPCyT (PICT-Serie A-02988), for financial support. D. M. G. is a member of the Research Career of CONICET.

Conflict of Interests

The authors declare no conflict of interest.

Data Availability Statement

The data that support the findings of this study are available in the Supporting Information of this article.

Keywords: Anagostic interaction · Crystal voids energy · Isostructurality · Phosphines · Steric descriptors

[1] a) Y. Kaya, A. Erçağ, A. Koca, *J. Mol. Struct.* **2020**, *1206*, 127653; b) M. Shabbir, Z. Akhter, A. R. Ashraf, H. Ismail, A. Habib, B. Mirza, *J. Mol. Struct.* **2017**, *1149*, 720–726; c) S. Güveli, B. Ülküseven, *Polyhedron* **2011**, *30*, 1385–1388; d) M. L. Clarke, J. J. R. Frew, *Organomet. Chem. RSC* **2009**, *35*, pp. 19–46.
[2] S. Naik, P. Parameswaranaik, N. S. Kumar, G. Krishnamurthy, K. S. J. Kumara, M. Somegowda, *Int. J. Biol. Med. Res.* **2018**, *9*, 6393–6399.
[3] J. J. Fernández, A. Fernández, D. Vázquez-García, M. López-Torres, A. Suárez, N. Gómez-Blanco, J. M. Vila, *Eur. J. Inorg. Chem.* **2007**, *34*, 5408–5418.
[4] a) M. Landman, T. Levell, P. H. van Rooyen, J. Conradie, *J. Mol. Struct.* **2014**, *1065-1066*, 29; b) J. Flapper, P. Wormald, M. Lutz, A. L. Spek, P. W. N. M. van Leeuwen, C. J. Elsevier, P. C. J. Kamer, *Eur. J. Inorg. Chem.* **2008**, *31*, 4968–4976.
[5] C. A. Tolman, *Chem. Rev.* **1977**, *77*, 313–348.
[6] a) G. Ferguson, P. J. Roberts, E. C. Alyea, M. Khan, *Inorg. Chem.* **1978**, *17*, 2965–2967; b) T. L. Brown, K. J. Lee, *Coord. Chem. Rev.* **1993**, *128*, 89–116; c) T. E. Müller, D. M. P. Mingos, *Transit. Met. Chem.* **1995**, *20*, 533–539; d) K. A. Bunten, L. Chen, A. L. Fernández, A. J. Poë, *Coord. Chem. Rev.* **2002**, *233-234*, 41–51; e) S. Otto, *Acta Crystallogr. Sect. C* **2001**, *57*, 793–795.
[7] J. A. Bilbrey, A. H. Kazez, J. Locklin, W. D. Allen, *J. Comput. Chem.* **2013**, *34*, 1189–1197.
[8] J. A. Bilbrey, W. D. Allen, *Annual Reports in Computational Chemistry*, Vol. *9*, **2013**, Elsevier, B.V.
[9] J. A. Bilbrey, A. H. Kazez, J. Locklin, W. D. Allen, *J. Chem. Theory Comput.* **2013**, *9*, 5734–5744.
[10] I. A. Guzei, M. Wendt, *Dalton Trans.* **2006**, 3991–3999.
[11] H. Novoa, H. Pérez, N. M. Blaton, O. M. Peeters, C. J. De Ranter, J. M. López, J. M. Moreno, *J. Chem. Crystallogr.* **2000**, *30*, 173–176.
[12] G. M. Ferrence, C. A. Tovee, S. J. W. Holgate, N. T. Johnson, M. P. Lightfoot, K. L. Nowakowska-Orzechowska, S. C. Ward, *IUCrJ* **2023**, *10*, 6–15.
[13] O. Seewald, U. Flörke, G. Henkel, *Acta Crystallogr. Sect. E* **2005**, *61*, 1829–1830.
[14] R. L. Carlin, R. D. Chirico, E. Sinn, G. Mennenga, L. J. de Jongh, *Inorg. Chem.* **1982**, *21*, 2218–2222.
[15] L. Brammer, E. D. Stevens, *Acta Crystallogr. Sect. C* **1989**, *45*, 400–403.
[16] J. A. J. Jarvis, R. H. B. Mais, P. G. Owston, *J. Chem. Soc. A* **1968**, 1473–1486.
[17] R. W. Humphry, A. J. Welch, D. A. Welch, *Acta Crystallogr. Sect. C* **1988**, *44*, 1717–1719.
[18] S. Vongtragool, B. Gorshunov, M. Dressel, J. Krzystek, D. M. Eichhorn, J. Telse, *Inorg. Chem.* **2003**, *42*, 1788–1790.
[19] D. Christendat, I. S. Butler, D. F. R. Gilson, R. Hynes, F. G. Morin, *Inorg. Chim. Acta* **2004**, *357*, 3775–3779.
[20] a) M. Brookhart, M. L. H. Green, *J. Organomet. Chem.* **1983**, *250*, 395–408; b) M. Brookhart, M. L. H. Green, G. Parkin, *Proc. Natl. Acad. Sci. USA* **2007**, *104*, 6908–6914; c) Y. Wenbin, O. Eisenstein, R. H. Crabtree, *Inorg. Chim. Acta* **1997**, *254*, 105–111.
[21] S. K. Singh, M. G. B. Drew, N. Singh, *Cryst. Eng. Comm.* **2013**, *15*, 10255–10265.
[22] E. Sathiyaraj, T. Srinivasan, S. Thirumaran, D. Velmurugan, *J. Mol. Struct.* **2015**, *1102*, 203–209.
[23] a) G. R. Desiraju, *Angew. Chem., Int. Ed.* **2011**, *50*, 52–59; b) M. M. Jotani, J. L. Wardell, E. R. T. Tiekink, *Z. Kristallogr.* **2018**, *233*, 675–690; c) R. M. Kumar, M. Elango, R. Parthasarathi, D. Vijay, V. Subramanian, *J. Chem. Sci.* **2012**, *124*, 193–202; d) D. Sadhukhan, M. Maiti, G. Pilet, A. Bauzá, A. Frontera, S. Mitra, *Eur. J. Inorg. Chem.* **2015**, 1958–1972; e) A. Bauzá, A. Frontera, *Angew. Chem. Int. Ed. Engl.* **2015**, *54*, 7340–7343.
[24] a) S. L. Tan, M. M. Jotani, E. R. T. Tiekink, *Acta Crystallogr. Sect. E* **2019**, *75*, 308–318; b) D. M. Gil, H. Pérez, G. A. Echeverría, O. E. Piro, A. Frontera, *ChemistrySelect* **2020**, *5*, 6331–6338; c) M. B. Fugu, J. Coley, I. F. Dickinson, J. B. Orton, W. Klooster, M. P. Gleeson, L. F. Jones, *CrystEngComm* **2021**, *23*, 5531–5539.
[25] P. R. Spackman, M. J. Turner, J. J. McKinnon, S. K. Wolff, D. J. Grimwood, D. Jayatilaka, M. A. Spackman, *J. Appl. Crystallogr.* **2021**, *54*, 1006–1011.
[26] A. G. P. Maloney, P. A. Wood, S. Parsons, *CrystEngComm* **2015**, *17*, 9300–9310.
[27] M. J. Turner, S. P. Thomas, M. W. Shi, D. Jayatilaka, M. A. Spackman, *Chem. Commun.* **2015**, *51*, 3735–3738.
[28] a) P. Bombicz, N. V. May, D. Fegyverneki, A. Saranchimeg, L. Bereczki, *CrystEngComm* **2020**, *22*, 7193–7203; b) A. Kálmán, L. Párkányi, G.y. Argay, *Acta Crystallogr. Sect. B* **1993**, *49*, 1039–1049; c) A. Kálmán, G. Argay, D. Scharfenberg-Pfeiffer, E. Höhne, B. Ribár, *Acta Crystallogr. Sect. B* **1991**, *47*, 68–77.
[29] L. Párkányi, ISOS Program, GUI Version 22.03.21, Compute isostructurality indices, Accesed Nov 22, 2024, http://www.chemcryst.hu/isos/.
[30] G. Bergerhoff, M. Berndt, K. Brandenburg, T. Degen, *Acta Crystallogr. Sect. B* **1999**, *55*, 147–156.
[31] E. S. Tasci, G. De La Flor, D. Orobengoa, C. Capillas, J. M. Pérez-Mato, M. I. Aroyo, *EPJ Web of Conferences* **2012**, *22*, 00009.
[32] J. Rohlíček, E. Skořepová, M. Babor, J. Čejka, *J. Appl. Crystallogr.* **2016**, *49*, 2172–2183.
[33] a) T. Gelbrich, M. B. Hursthouse, *CrystEngComm* **2005**, *7*, 324–336; b) T. Gelbrich, M. B. Hursthouse, *CrystEngComm* **2006**, *8*, 448–460; c) F. P. A. Fabbiani, B. Dittrich, A. J. Florence, T. Gelbrich, M. B. Hursthouse, W. F. Kuhs, N. Shankland, H. Sowa, *CrystEngComm* **2009**, *11*, 1396–1406; d) T. Gelbrich, T. L. Threlfall, M. B. Hursthouse, *CrystEngComm* **2012**, *14*, 5454–5464.
[34] a) J. J. McKinnon, D. Jayatilaka, M. A. Spackman, *Chem. Commun.* **2007**, 3814–3816; b) M. A. Spackman, D. Jayatilaka, *CrystEngComm* **2009**, *11*, 19–32.
[35] P. R. Spackman, M. J. Turner, J. J. McKinnon, S. K. Wolff, D. J. Grimwood, D. Jayatilaka, M. A. Spackman, *J. Appl. Crystallogr.* **2021**, *54*, 1006–1011.
[36] a) M. J. Turner, J. J. McKinnon, D. Jayatilaka, M. A. Spackman, *CrystEngComm* **2011**, *13*, 1804–1813; b) K. M. Chandini, M. J. N. Khadri, N. Amoghavarsha, M. A. Sridhar, S. A. Khanum, *Heliyon* **2022**, *8*, e10047.
[37] a) J. Contreras-García, E. R. Johnson, S. Keinan, R. Chaudret, J.-P. Piquemal, D. N. Beratan, W. Yang, *J. Chem. Theory Comput.* **2011**, *7*, 625–

632; b) E. R. Johnson, S. Keinan, P. Mori-Sánchez, J. Contreras-García, A. J. Cohen, W. Yang, *J. Am. Chem. Soc.* **2010**, *132*, 6498–6506.

[38] W. Humphrey, A. Dalke, K. Schulten, *J. Mol. Graphics* **1996**, *14*, 33–38.

[39] T. Williams, C. Kelley, GNUPLOT v. 5.2: An Interactive Plotting Program.

[40] a) A. Gavezzotti, *New J. Chem.* **2011**, *35*, 1360–1368; b) A. Gavezzotti, *J. Phys. Chem. B* **2003**, *107*, 2344–2353; c) A. Gavezzotti, *J. Phys. Chem. B* **2002**, *106*, 4145–4154.

[41] M. J. Frisch, G. W. Trucks, H. B. Schlegel, G. E. Scuseria, M. A. Robb, J. R. Cheeseman, G. Scalmani, V. Barone, G. A. Petersson, H. Nakatsuji, X. Li, M. Caricato, A. Marenich, J. Bloino, B. G. Janesko, R. Gomperts, B. Mennucci, H. P. Hratchian, J. V. Ortiz, A. F. Izmaylov, J. L. Sonnenberg, D. Williams-Young, F. Ding, F. Lipparini, F. Egidi, J. Goings, B. Peng, A. Petrone, T. Henderson, D. Ranasinghe, V. G. Zakrzewski, J. Gao, N. Rega, G. Zheng, W. Liang, M. Hada, M. Ehara, K. Toyota, R. Fukuda, J. Hasegawa, M. Ishida, T. Nakajima, Y. Honda, O. Kitao, H. Nakai, T. Vreven, K. Throssell, J. A. Montgomery, Jr., J. E. Peralta, F. Ogliaro, M. Bearpark, J. J. Heyd, E. Brothers, K. N. Kudin, V. N. Staroverov, T. Keith, R. Kobayashi, J. Normand, K. Raghavachari, A. Rendell, J. C. Burant, S. S. Iyengar, J. Tomasi, M. Cossi, J. M. Millam, M. Klene, C. Adamo, R. Cammi, J. W. Ochterski, R. L. Martin, K. Morokuma, O. Farkas, J. B. Foresman, D. J. Fox, Gaussian 16 (Revision A.03), Gaussian Inc., Wallingford, CT, **2016**.

[42] a) C. Adamo, V. Barone, *J. Chem. Phys.* **1999**, *110*, 6158–6170; b) S. Grimme, J. Antony, S. Ehrlich, H. Krieg, *J. Chem. Phys.* **2010**, *132*, 154104; c) F. Weigend, *Phys. Chem. Chem. Phys.* **2006**, *8*, 1057–1065.

[43] R. F. W. Bader, *Chem. Rev.* **1991**, *91*, 893–928.

[44] T. Lu, F. Chen, *J. Comput. Chem.* **2012**, *33*, 580–592.

[45] a) E. D. Glendening, C. R. Landis, F. Weinhold, *J. Comput. Chem.* **2019**, *40*, 2234–2241; b) NBO 7.0. E. D. Glendening, J. K. Badenhoop, A. E. Reed, J. E. Carpenter, J. A. Bohmann, C. M. Morales, P. Karafiloglou, C. R. Landis, F. Weinhold, Theoretical Chemistry Institute, University of Wisconsin, Madison **2018**.

[46] L. E. Manzer, C. A. Tolman, *J. Am. Chem. Soc.* **1975**, *97*, 1955–1956.

[47] a) H. Pérez, R. Ramos, A. M. Plutín, R. Mocelo, M. F. Erben, E. E. Castellano, A. A. Batista, *Eur. J. Inorg. Chem.* **2019**, 2583–2590; b) P. Lakshmanan, E. Sathiyaraj, S. Thirumaran, S. Ciattini, *Phosphorus, Sulfur Silicon Relat. Elem.* **2021**, *196*, 622–633; c) K. K. Manar, A. N. Gupta, A. K. Gupta, L. B. Prasad, P. Srivastava, M. G. B. Drew, N. Singh, *ChemistrySelect* **2017**, *2*, 2655–2664; d) A. P. Balasubramaniam, A. Peuronen, M. Lahtinen, M. Manickavachagam, E. Kolehmainen, E. Haapaniemi, M. Sillanpaa, *Polyhedron* **2017**, *123*, 453–461.

[48] F. H. Allen, I. J. Bruno, *Acta Crystallogr. Sect. B* **2010**, *66*, 380–386.

[49] O. V. Dolomanov, L. J. Bourhis, R. J. Gildea, J. A. K. Howard, H. Puschmann, *J. Appl. Crystallogr.* **2009**, *42*, 339–341.

[50] H. H. Al Mamari, Y. Al Lawati, *J. Chem. Res.* **2020**, *44*, 705–709.

[51] H. Novoa, H. Pérez, O. M. Peeters, N. Blaton, C. De Ranter, J. M. López, *Acta Crystallogr. Sect. C* **2000**, *56*, e98–e99.

[52] Y. Zhang, J. C. Lewis, R. G. Bergman, J. A. Ellman, E. Oldfield, *Organometallics* **2006**, *25*, 3515–3519.

[53] W. Levason, D. Pugh, G. Reid, *Acta Crystallogr. Sect. C* **2013**, *69*, 560–564.

[54] A. L. Spek, *Acta Crystallogr. Sect. D* **2009**, *65*, 148–155.

[55] I. Dance, *New J. Chem.* **2003**, *27*, 22–27.

[56] a) A. Saeed, Z. Ashraf, J. Simpson, H. Pérez, M. F. Erben, *J. Mol. Struct.* **2019**, *1195*, 796–806; b) N. Shamsudin, A. L. Tan, D. J. Young, M. M. Jotani, A. Otero-de-la-Roza, E. R. T. Tiekink, *Acta Crystallogr. Sect. E* **2016**, *72*, 563–569.

[57] C. F. Macrae, I. J. Bruno, J. A. Chisholm, P. R. Edgington, P. McCabe, E. Pidcock, L. R. Monge, R. Taylor, J. van de Streek, A. Wood, *J. Appl. Crystallogr.* **2008**, *41*, 466–470.

[58] Y. Zhang, J. C. Lewis, R. G. Bergman, J. A. Ellman, E. Oldfield, *Organometallics* **2006**, *25*, 3515–3519.

[59] a) M. Hamel, M. Lecinq, M. Gulea, J. Kozelka, *J. Organomet. Chem.* **2013**, *206*, 745–746; b) R. F. W. Bader, *Atoms in Molecules: A Quantum Theory*, Oxford University Press, Oxford, UK, **1990**.

[60] E. Espinosa, E. Molins, C. Lecomte, *Chem. Phys. Lett.* **1998**, *285*, 170–173.

[61] E. Bartashevich, S. Mukhitdinova, I. Yushina, V. Tsirelson, *Acta Crystallogr. Sect. B Struct. Sci. Cryst. Eng. Mater.* **2019**, *75*, 117–126.

Manuscript received: September 30, 2024